Efficient Calculation of Charge-Transfer Matrix Elements for Hole Transfer in DNA

Tomáš Kubař,[†] P. Benjamin Woiczikowski,[†] Gianaurelio Cuniberti,[‡] and Marcus Elstner*[,†,§]

Department of Physical and Theoretical Chemistry, Technische Universität Braunschweig, D-38106 Braunschweig, Germany, Institute for Materials Science and Max Bergmann Center of Biomaterials, Technische Universität Dresden, D-01062 Dresden, Germany, and Department of Molecular Biophysics, German Cancer Research Center, D-69115 Heidelberg, Germany

Received: February 19, 2008; Revised Manuscript Received: April 3, 2008

We present a new computational strategy to evaluate the charge-transfer (CT) parameters for hole transfer in DNA. On the basis of a fragment-orbital approach, site energies and coupling integrals for a coarse-grained tight-binding description of the electronic structure of DNA are rapidly calculated using the approximative density functional method SCC-DFTB. The methodology is validated by extensive test calculations in comparison with DFT and ab initio reference data, demonstrating its high accuracy at low computational cost. Environmental effects are captured using a quantum mechanics−molecular mechanics (QM/MM) coupling scheme, and dynamical effects are included by evaluating the CT parameters along classical molecular dynamics simulations. This combined methodology allows for a realistic treatment of CT processes in DNA.

I. Introduction

The ability of natural double-stranded DNA (dsDNA) to transfer electric charge over long distances has attracted much interest in the past decade. Many chemical studies were conducted in order to understand the fundamental mechanism of charge transfer (CT) in DNA,[1] which may also be involved in the repair of oxidatively generated damage.[2,3] Experiments performed mainly in the physics community attempted to probe the ability of DNA to serve as a molecular wire for molecular electronics applications.[4–6] The wide spectrum of contradictory results obtained may be ascribed to the complex character of DNA and to the very sensitive dependence of its electrical response on internal and environmental degrees of freedom, as well as on the substrate anchoring. Despite immense experimental and theoretical efforts, basic problems regarding DNA conductivity remain unresolved. This mainly concerns the transport mechanisms and, strongly related to that, the *intrinsic conductivity* of DNA.

Early proposals based on the ideas of Eley and Spivey[7] suggested that the π molecular orbitals of DNA bases form extended bands along the DNA strand, and DNA might then act as a one-dimensional aromatic crystal. However, theoretical studies demonstrated that DNA does not support the extended-orbital picture.[4,8,9] Two distinct mechanistic regimes of charge transfer have been shown to occur in DNA; over short distances, the fully coherent transfer features an exponential distance dependence,[10,11] theoretically described by the superexchange model.[12–17] On the other hand, charge transfer over long distances has been reported,[18–21] and its weak distance dependence cannot be rationalized as a single superexchange event. Then, the charge transfer may be modeled as a multistep hopping process between guanine (G) bases mediated by tunneling through adenine−thymine (AT) bridges with an algebraic distance dependence.[13,22–25] For longer AT bridges, an A-hopping[10] mechanism has been proposed, that is, the hole is thermally activated from G to A bases and may travel via single-step hopping events along the A tracts, theoretically described as thermally induced hopping (TIH) process.[26–30] The crossover of the mechanism due to the elongation of the AT bridge was supported experimentally.[31–33]

The energetics of the CT process is determined by the redox potential of the bases, which has been measured in the gas phase[34,35] or estimated in water.[36] Thus, most theoretical attempts (usually based on static DNA structures) modeled the CT in DNA using two sets of parameters, also called CT matrix elements: the ionization potentials (IP) of the individual bases and the electronic coupling matrix elements T_{ij} between the localized states on the respective donor (i) and acceptor (j) nucleobases. The radical cation state is roughly 0.4 eV more stable on G than that on A, while the C and T radical cation states are separated from G by more than 1 eV. Therefore, it is very unlikely for a hole to be localized on the C or T bases. Concerning the transfer of holes between donor and acceptor sites, the rate of nonadiabatic CT is determined by the CT matrix element and the thermally weighted Franck−Condon (FC) factor[37]

$$k = \frac{2\pi}{\hbar}|T_{ij}|^2 \times \mathrm{FC} \tag{1}$$

Therefore, the relative energies of radical cation states (entering the FC term) and the electronic couplings are the key parameters to describe CT in the tunneling regime as well as in the incoherent hopping regime, where the hopping rates between neighboring bases are calculated in the same fashion. Also, these parameters can be cast into the form of a tight-binding-like Hamiltonian

$$\hat{H} = \sum_i \epsilon_i \hat{a}_i^+ \hat{a}_i + \sum_{ij} T_{ij} \hat{a}_i^+ \hat{a}_j \tag{2}$$

with ϵ_i representing the IP values of respective bases. Such Hamiltonians have been used to solve the time-dependent Schrödinger equation, to compute hole-transfer rates,[24,38,39] or to parametrize a Su-Schrieffer-Heeger (SSH) type Hamiltonian.[40–42]

* To whom correspondence should be addressed. E-mail: m.elstner@tu-bs.de. Phone: +49-531-3915347. Fax: +49-531-3915832.
[†] Technische Universität Braunschweig.
[‡] Technische Universität Dresden.
[§] German Cancer Research Center.

10.1021/jp801486d CCC: $40.75
Published on Web 06/11/2008

In the physics community, tight-binding Hamiltonians are widely applied to compute the transmission or electrical currents through DNA (for recent reviews, see refs 43 and 44). All of these models depend on an appropriate choice of parameters. Usually, they use CT parameters computed for fixed geometries, either completely neglecting the environmental effects or only partially including them, mostly on the basis of continuum approaches (e.g., see refs 40 and 45). The same is true for the tight-binding methods, although the dynamical effects like electron−phonon coupling and coupling to the bath are modeled in a parametrized way. However, the necessary parameters are difficult to determine accurately.[43,44]

Several theoretical approaches were developed which allow for a description of CT over fluctuating bridges.[46–48] The implementation of such methodologies usually involved a combination of classical MD simulation with semiempirical quantum chemistry and constituted a basis to assess the solvent effect on CT and to deduce the CT mechanism in organic molecules and proteins.[49–52] For hole transfer in DNA, it has been shown that the fluctuations of parameters due to dynamical effects and environmental interactions may have significant impact: the CT parameters exhibit large oscillations when computed for snapshots along classical MD trajectories.[53–55] However, so far, these effects have not been included in the theoretical description of CT in DNA in a rigorous way, and the simulations of dynamical effects were based on simple models.[38,39,56,57] Thus far, a realistic description of solvation effects on the diagonal terms T_{ii} has been given merely by Voityuk et al.,[58] who performed classical MD simulations and quantified the fluctuation of T_{ii} (or IP's) in a quantum mechanics−molecular mechanics (QM/MM) framework. The results show large-scale fluctuations of T_{ii}, not considered in any of the models up to now, which definitely have an overwhelming impact on the dynamics of hole transfer and the conduction in DNA wires.

In particular, the interpretation of several experiments focuses on the impact of structural fluctuations and environmental interactions, as compiled in refs 59 and 60. In contrast to the TIH model, which presupposes a hole localized on one site (one DNA base), the hole is assumed to be delocalized over several sites. Summarizing several recent experiments, Barton emphasizes structural fluctuations facilitating the hole transfer, suggesting DNA to be in a "CT-active conformation", where the couplings between sites (T_{ij}) tend to be maximized[59,61] (conformational gating model). Schuster discusses experimental findings, which cannot be rationalized in terms of a localized hole. The environment seems to modify the properties of a site significantly, and the experiments are described in terms of a polaron hopping. In addition, the effect of counterion motion on CT is highlighted (ion gating mechanism), which has already been illustrated by quantum-mechanics calculations.[62] The simulations of Conwell[40] pick up on the polaron model and show the importance of water polarization, however without explicit treatment of counterions in the model. The importance of water motion has also been reported in a recent quantum mechanics simulation.[63]

These findings emphasize the importance of proper inclusion of dynamical and solvent effects into the theoretical description of CT in DNA, which should be based on an accurate scheme for the calculation of CT parameters. In all of these models, the electronic structure of DNA is usually treated at a "coarse-grained" level, that is, the transport between the highest occupied molecular orbitals (HOMO) of neighboring bases is considered. Then, the Hamiltonian in eq 2 constitutes an efficient way of "coarse graining" of the computational problem, with only the HOMOs of involved purine bases being considered as building blocks of the DNA electronic structure.

The required electronic couplings T_{ij} can be computed in various ways.[37] Most frequently, the T_{ij} have been estimated by calculating the energy splitting of adiabatic states; for a recent review, see ref 64. A simple and efficient approach is to approximate this energy splitting by the difference of HF one-electron energies using the Koopmans theorem approximation (KTA).[65,66] In the same way, the couplings can also be calculated using density functional theory (DFT).[17] However, the HF-KTA approximation was shown to overestimate the couplings significantly, and the treatment on a higher CAS-PT2 level of theory reduces the value of couplings by up to 40%.[67] These CAS-PT2 reference calculations can be considered as an accurate benchmark for more approximating methods.

In the fragment-orbital (FO) approach, the couplings are calculated directly from the diabatic states ϕ_i and ϕ_j located on the donor and acceptor sites. In practice, these predetermined states are approximated as the HOMO orbitals on two adjacent bases, and the matrix elements $T_{ij} = \langle\phi_j|\hat{H}|\phi_j\rangle$ and $S_{ij} = \langle\phi_i|\phi_j\rangle$ can be calculated with either HF or DFT, using either the Fock operator[68] or the Kohn−Sham Hamiltonian[39] for $\hat{H}$. Usually, these orbitals are calculated separately for isolated DNA bases since they are not significantly modified by the interactions within Watson−Crick pairing.[68] Then, the conformational specificity enters the stage just via the molecular Hamiltonian (Fock operator) $\hat{H}$. Rak et al.[69] showed that the methods based on adiabatic and diabatic states lead to comparable numerical values.

In the HF-KTA and FO approaches, usually only the two donor and acceptor bases are treated explicitly, that is, environmental effects are neglected completely. Interactions with the environment are at least partially covered by methods that consider large DNA fragments for the calculation of couplings, using orbital localization[70,71] or block diagonalization[72] techniques, but at a much higher computational cost.

The combination of an accurate treatment of the quantum problem with a proper account of dynamical and environmental effects points toward the implementation of an appropriate quantum mechanics−molecular mechanics (QM/MM) framework, which has become a standard for this kind of problems in the past decade (for a comprehensive review, see ref 73). In the context of CT through DNA, this approach allows for a systematic coarse graining from the atomistic level. In the first step, extended molecular dynamics (MD) simulations of DNA oligomers are performed to ensure sufficiently long sampling times. In the second step, the couplings and the site energies are calculated along these trajectories, thereby including the dynamical effects naturally while additionally incorporating the electrostatic interactions with the DNA backbone and solvent environment of the bases.

In this work, we present such a combined coarse-grained scheme, where the computation of CT parameters is based on the approximating self-consistent-charge density functional tight-binding method (SCC-DFTB).[74] This methodology will allow the study of the charge-transfer processes in DNA and related molecules in a realistic fashion. In this work, we first describe the SCC-DFTB-based technique for the calculation of CT parameters. Then, we benchmark the method with respect to higher-level methods, and finally, we illustrate the concept with applications to static structures and MD simulation of DNA in solution.

II. Methodology

A. The Fragment-Orbital Approach. The fragment-orbital (FO) approach allows for a direct and well-controlled coarse graining of the electronic problem. Since the hole transfer in DNA occurs between the HOMOs ϕ_i and ϕ_j of individual DNA bases i and j, the electronic Hamiltonian of the system can be formulated in terms of the on-site energies of those nucleobases (representing the diagonal elements: $T_{ii} = \epsilon_i$) and the CT (coupling) integrals between the sites i and j (giving the off-diagonal elements T_{ij}). The orbitals ϕ_i can be obtained by treating only fragments of the whole system, therefore called fragment orbitals (FO). In the case of DNA, these fragments can be chosen as isolated bases or Watson−Crick (WC) base pairs. The diagonal terms $T_{ii} = \epsilon_i$ can be calculated as

$$\epsilon_i = -\langle \phi_i | \hat{H}_{KS} | \phi_i \rangle \tag{3}$$

and the coupling integrals can be evaluated with the Kohn−Sham Hamiltonian $\hat{H}_{KS}$ of the respective base pair, using the FOs

$$T_{ij} = \langle \phi_i | \hat{H}_{KS} | \phi_j \rangle \tag{4}$$

Applying the atomic basis set expansion

$$\varphi_i = \sum_\mu c_\mu^i \eta_\mu \tag{5}$$

the coupling and overlap integrals in the molecular orbital (MO) basis can be efficiently evaluated as

$$T_{ij} = \sum_{\mu\nu} c_\mu^i c_\nu^j \langle \eta_\mu | \hat{H}_{KS} | \eta_\nu \rangle = \sum_{\mu\nu} c_\mu^i c_\nu^j H_{\mu\nu} \tag{6}$$

and

$$S_{ij} = \sum_{\mu\nu} c_\mu^i c_\nu^j \langle \eta_\mu | \eta_\nu \rangle = \sum_{\mu\nu} c_\mu^i c_\nu^j S_{\mu\nu} \tag{7}$$

$H_{\mu\nu}$ and $S_{\mu\nu}$ are the Hamilton and overlap matrices represented in the atomic basis set. These matrices and the atomic coefficients c_μ^i can be determined by HF or DFT calculations on the molecular fragments, where the HOMOs are located, as discussed below. In this work, we use the matrix elements evaluated from SCC-DFTB.[74]

The matrix T_{ij} is built from nonorthogonal orbitals ϕ_i and ϕ_j. For many problems, a representation in an orthogonal basis set is more suitable, which can be achieved using the Loewdin transformation[75]

$$T_{ij}' = T_{ij} - S_{ij}(T_{ii} + T_{jj})/2 \tag{8}$$

In the following, T_{ij}' will denote the matrix based on the orthonormal basis, while T_{ij} is the matrix in nonorthonormal representation. The T_{ij}' can be identified with CT integrals computed, for example, using HF-KTA.[37]

B. The SCC-DFTB Method. In this work, we use the SCC-DFTB method to calculate the coupling matrix elements. Therefore, we review its formalism shortly.[74,76–79] SCC-DFTB is an approximate method, which is derived by a second-order expansion of the total DFT energy expression, followed by an approximation of the charge density fluctuations by charge monopoles and an effective damped Coulomb interaction between the net atomic charges. The total energy can be written as[74]

$$E^{SCC} = \sum_{i\mu\nu} c_\mu^i c_\nu^i H_{\mu\nu}^0 + \frac{1}{2}\sum_{\alpha\beta} \gamma_{\alpha\beta} \Delta q_\alpha \Delta q_\beta + \frac{1}{2}\sum_{\alpha\beta} U_{\alpha,\beta} \tag{9}$$

The introduction of minimal atomic orbital (AO) basis according to eq 5 leads to the Hamilton matrix $H_{\mu\nu}^0$ with the MO expansion coefficients c_μ^i, $\gamma_{\alpha\beta}$ represents the effective damped Coulomb interaction between the atomic charges Δq_α, and $U_{\alpha,\beta}$ is the repulsive two-body potential between the atoms α and β.

$H_{\mu\nu}^0$ is calculated using an optimized LCAO basis set η_μ. These basis functions are derived from atomic DFT calculations but are slightly confined due to the presence of an additional harmonic potential in the atomic Kohn−Sham equations[76]

$$\left[-\frac{1}{2}\nabla^2 + v_{eff}[\rho_{atom}] + \left(\frac{r}{r_0}\right)^2\right] \eta_\mu = \epsilon_\mu \eta_\mu \tag{10}$$

The confining potential drives a slight compression of atomic-like orbitals η_μ and atomic electronic densities ρ_α. Whereas such confined orbitals are favorable for many molecular and solid-state applications,[76] they may not be adequate for applications where more diffuse basis sets are needed, for example, the calculation of coupling integrals. With the basis functions and atomic densities, the overlap and Hamilton matrices

$$S_{\mu\nu} = \langle \eta_\nu | \eta_\mu \rangle \tag{11}$$

$$H_{\mu\nu}^0 = \langle \eta_\nu | \hat{H}[\rho_\alpha + \rho_\beta] | \eta_\mu \rangle \tag{12}$$

can be calculated for all necessary combinations of orbitals η_ν and η_μ on atoms α and β and stored in tables. Therefore, no further integral evaluation is needed during a SCC-DFTB run, which makes this method roughly two to three orders of magnitude faster than standard DFT methods.

The application of the variational principle to the total energy (eq 9) leads to a generalized eigenvalue problem, which has to be solved iteratively for the MO coefficients c_μ^i because the Hamilton matrix elements depend on the c_μ^i via the Mulliken charges ($\mu \in \alpha$, $\nu \in \beta$)

$$H_{\mu\nu}^{\alpha\beta} = H_{\mu\nu}^{0\alpha\beta} + \frac{1}{2} S_{\mu\nu}^{\alpha\beta} \sum_\delta \Delta q_\delta (\gamma_{\alpha\delta} + \gamma_{\beta\delta}) \tag{13}$$

These SCC-DFTB Hamilton and overlap matrix elements are used to calculate the coupling matrix elements (eq 6), producing a very efficient scheme as the matrix elements are read in from tables for every geometry, and no integral evaluations have to be performed anymore.

For such large molecular systems as DNA in solution, quantum chemical calculations become prohibitively expensive. A popular approach is to combine a quantum mechanics description (QM) of a small part of the system with a molecular mechanics treatment (MM) of the remainder of the system; for a recent comprehensive review see ref 73. Here, the QM subsystem is polarized by the surrounding MM charges Q_A.

In SCC-DFTB, the effect of external charges Q_A on the electronic structure can be accounted for using the QM/MM coupling to the Hamilton matrix elements[80]

$$H_{\mu\nu} = H_{\mu\nu}^0 + \frac{1}{2} S_{\mu\nu}^{\alpha\beta} \left(\sum_\delta \Delta q_\delta (\gamma_{\alpha\delta} + \gamma_{\beta\delta}) + \sum_A Q_A \left(\frac{1}{r_{A\alpha}} + \frac{1}{r_{A\beta}} \right) \right) \tag{14}$$

Using this equation, the influence of atomic charges from the DNA backbone, water molecules, and counterions as represented by an empirical force field can be taken into account directly. There are several options to calculate the coupling matrix elements. In the first step, the c_μ^i in eq 6 have to be calculated. As suggested above, this can be done by calculating the FOs for isolated fragments (bases or WC base pairs) using SCC-DFTB. Alternatively, the FOs can be computed for the fragments in the presence of point charges representing the environment. In the latter case, the effect of the environment is already

TABLE 1: IP of Nucleobases Calculated As ΔSCF and ϵ_{HOMO} using DFT and HF Methods (the 6-31G* basis set used)[a]

	guanine		adenine		cytosine		thymine	
method	ΔSCF	ϵ_{HOMO}	ΔSCF	ϵ_{HOMO}	ΔSCF	ϵ_{HOMO}	ΔSCF	ϵ_{HOMO}
DFTB	7.74	4.96	8.12	5.29	8.82	5.17	9.03	5.92
B3LYP	7.53	5.51	7.96	5.89	8.35	6.13	8.72	6.57
PBE	7.36	4.69	7.81	5.06	8.20	5.18	8.48	5.63
HF	−	7.99	−	8.37	−	9.16	−	9.52
NDDO-G[93]	8.10		8.53		9.10		9.15	
exp., vert.[34]	8.24		8.44		8.94		9.14	
exp., adiab.[35]	7.77		8.26		8.68		8.87	

[a] The NDDO-G as well as experimental values (vertical and adiabatic) are given for reference.

incorporated in the c_μ^i. In the second step, the AO Hamilton matrix is constructed in order to calculate the T_{ij} in eq 6. Again, this can be done in the absence or presence of the point charges representing the environment, that is, by either using the pure SCC-DFTB Hamiltonian (eq 13) or the QM/MM Hamiltonian (eq 14). In the latter case, the influence of the environment is fully accounted for in the Hamiltonian, which is probably even more important than that for the calculation of MO coefficients c_μ^i.

III. Tests of the DFTB-FO Parametrization

In a first step, we evaluate the DFTB-derived charge-transfer parameters for their application to hole transfer in DNA. This concerns the on-site elements $T_{ii} \equiv \epsilon_i$, which govern the energetics of charge transfer, as well as the coupling matrix elements T_{ij}, with the latter ones being sensitive to the choice of AO basis. The standard SCC-DFTB uses a confined basis set, with the confinement radius (eq 10) set to approximately twice the covalent radius of the respective atom.[74,77] The relaxation of this constraint leads to more diffuse basis functions and makes the coupling matrix elements more appropriate, as described below.

A. Ionization Potentials and On-Site Energies. The energetics of hole transfer between two nucleobases can be estimated from the difference of the IP of these molecules. Therefore, the first important step is to benchmark SCC-DFTB in this respect. Table 1 compares the vertical IP values calculated with HF-KTA with those determined with B3LYP, PBE (using Gaussian03[81]), and DFTB using the ΔSCF procedure. The vertical IPs are slightly underestimated by both DFT functionals as well as SCC-DFTB (using the standard basis), which even gives the best agreement with the experimental values. Further, the SCC-DFTB values agree perfectly with the experimental adiabatic IP. In particular, the relative energies, which are important for the energetics of hole transfer in DNA, are quite well reproduced. Therefore, SCC-DFTB is well suited for the simulation of CT processes in this respect.

The calculation of the Kohn−Sham single-particle HOMO energy is a faster way to estimate the on-site energy than using the ΔSCF procedure. However, several problems arise when using approximative DFT functionals based on the generalized gradient approximation (GGA). First of all, the HOMO energies are significantly underestimated. While the HOMO energy represents the adiabatic IP value quite well with HF due to Koopman's theorem, it does not match if using GGA or hybrid functionals like PBE or B3LYP, as a consequence of the wrong asymptotic behavior of GGA exchange functionals. Since SCC-DFTB is parametrized to PBE, this holds for SCC-DFTB as well, as can be seen from Table 1. Actually, it is only the relative HOMO energies of individual bases that affect the CT process, and the HOMO energy difference provided by SCC-DFTB is correct for guanine and adenine, making this shortcoming irrelevant.

Also, the cytosine HOMO energy is severely underestimated with respect to adenine and guanine by all DFT methods. Nevertheless, the actually high-lying HOMO of cytosine and thymine will prevent a hole from being localized on these bases. Thus, the C and T bases may be excluded from the quantum chemical description without loss of accuracy, and we do not aim at evaluating the site energy of pyrimidine bases in any applications. This way, the DFT failure becomes irrelevant. As can be seen from the table, the relative energies of adenine and guanine are well reproduced by both HOMO energies and ΔSCF values for all of the DFT methods. In this case, the SCC-DFTB Kohn−Sham energies can be used as an approximation of the energy of a hole residing on a particular nucleobase.

Another point of imperfection represents the energy difference between the HOMO and the second-highest occupied MO (HOMO-1) being too small in some cases, as can be seen in the tables in the Supporting Information section. (For cytosine, HOMO and HOMO-1 may even swap with DFT, depending on minor changes in the molecular geometry.) The HOMO − HOMO-1 energy difference of less than 0.4 eV is problematic, as fluctuations of this magnitude appear typically during MD simulations, as discussed below, and consequently, the orbitals with such small energy difference may change order in the course of MD simulation. Since HOMO-1 of both guanine and adenine has σ character in DFT, a wrong representation of the electronic structure would result. The hybrid functional B3LYP alleviates this problem slightly due to the HF content; yet, a HOMO − HOMO-1 energy difference of less than 0.4 eV still appears.

Interestingly, the inclusion of solvent water in the calculation seems to reduce this effect considerably, as shown, for example, by York et al.[82] Much the same, when both the FOs and the CT integrals are computed in the presence of external point charges representing the DNA backbone, water, and counterions, the energy difference becomes much larger, and the artificial level crossings disappear.

B. A DFTB Basis Set Optimized for Hole Transfer. The standard basis set for DFTB is constructed by using eq 10 with rather small values of r_0. Usually, r_0 for an atomic orbital is chosen to be twice the covalent radius of the element, yielding typical values for carbon, nitrogen, and oxygen between 2 and 3 au. This, however, leads to rather small coupling integrals T_{ij} (eq 4), as the important wave function tails are suppressed using such a confined basis. Therefore, we relaxed the tight confinement radius for the basis functions η_μ. The calculation of DFTB Hamilton matrix elements (eq 12) consists of two steps. First, the electronic density on atoms is calculated from eq 10 using a constant value of $r_0 = 7.0$ au (for a more detailed discussion, see ref 77). In the second step, the basis functions are η_μ using a different value of the confinement radius r_0. The dependence of T_{ij} (eq 4) and T_{ij}' (eq 8) on r_0 for the basis function is shown in Figure 1 (with $r_0 = 7.0$ au for the density).

T_{ij} is constantly increasing with increasing r_0, while T_{ij}' assumes a maximum at r_0 at around 8 au. This is due to the effect of increased overlap S_{ij}, which seems to overrule the r_0 dependence of T_{ij}, according to eq 8, thereby making T_{ij}' drop slightly for large r_0. More extensive tests showed that the values $r_0(\text{dens}) = 7$ au and $r_0(\text{wf}) = 8$ au lead to quite a good agreement with higher-level calculations. These fixed values

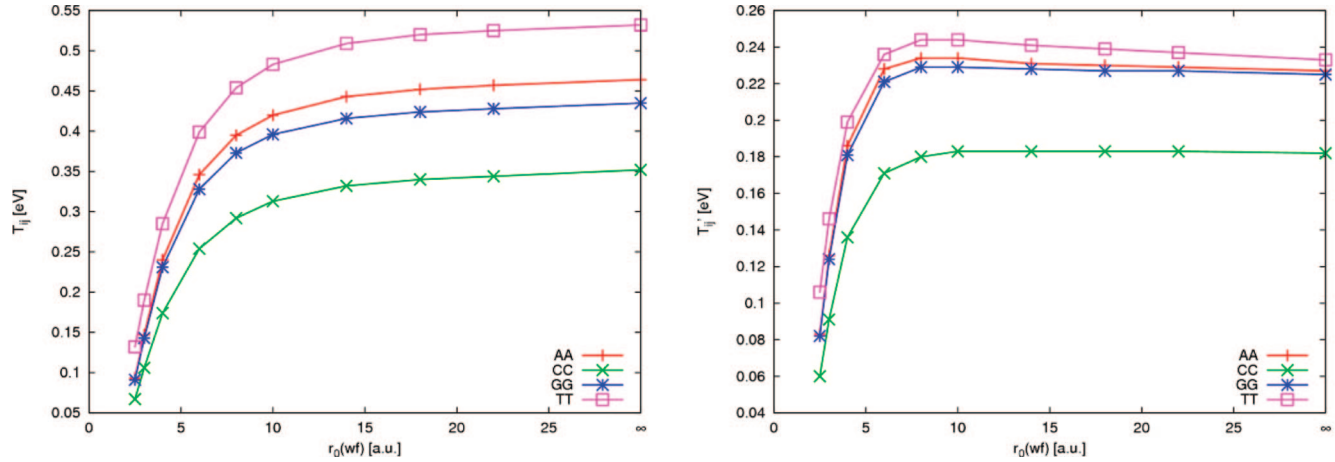

Figure 1. T_{ij} (left) and T_{ij}' (right) with respect to r_0(wf) using r_0(dens) = 7 au for stacked base pairs adenine−adenine (AA), cytosine−cytosine (CC), guanine−guanine (GG), and thymine−thymine (TT) (in the configuration with rise = 3.38 Å and twist = 0°).

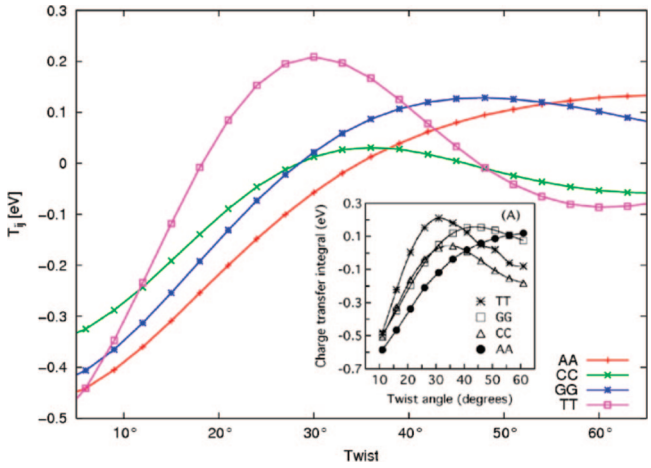

Figure 2. T_{ij} with respect to the twist angle (with helical parameter rise 3.38 Å) for stacked pairs adenine−adenine (AA), cytosine−cytosine (CC), guanine−guanine (GG), and thymine−thymine (TT) (inset shows the corresponding DFT results from ref 39).

(from now on called the "8−7 basis set") will be applied to compute the DFTB matrix elements as used in this work.

Senthilkumar et al.[39] evaluated CT integrals using DFT based on the FO approach as discussed above. They determined HOMOs ϕ_i for isolated nucleobases and calculated the CT integrals using the Kohn−Sham Hamiltonian for the stacked nucleobase dimer: $T_{ij} = \langle \phi_i | \hat{H}_{KS} | \phi_j \rangle$. We use exactly the same approach as that outlined above but use the much faster approximative SCC-DFTB rather than the full DFT-SCF as used in ref 39. Thus, the mentioned work represents an excellent benchmark for our method. Figure 2 shows the dependence of T_{ij} on the twist parameter of a base pair step at a constant distance ("rise") of 3.38 Å, the bases assuming a parallel configuration. The DFTB values match very well with the DFT data (inset from ref 39); especially the qualitative and quantitative differences between the base pairs are reproduced excellently. Only for small twist angles are the DFTB values underestimated slightly.

The CT integrals have been calculated at various levels of theory in the recent years, mostly using HF-KTA as reviewed recently.[64] Interestingly, the HF values seem to be overestimated by 40% when compared with the values calculated on the more accurate CAS-PT2 level.[67] The latter calculations provide an excellent benchmark for other methods and explain the difference between HF and DFT values.[39] For comparison with the ab initio data, the CT integrals T_{ij}' have to be used. As shown in Table 2, the T_{ij}' calculated by DFTB agree quite well with the CAS-PT2 data,[67] while the larger T_{ij} data resemble the (overestimated) HF values nicely. In general, this holds for the DFT values in ref 39 as well; the nonorthogonal CT integrals J are larger than the orthogonalized J'. Anyways, the DFT values do not seem to match better with the CAS-PT2 reference than the SCC-DFTB ones do. This illustrates the challenging character of CT integral calculations, in particular for the B-DNA geometries, where these quantities take small values.

In summary, the DFTB-based CT integrals agree well with the accurate CAS-PT2 values, being smaller in magnitude than the widely used HF-based values. Therefore, DFTB can be used for a rapid and reliable evaluation of CT integrals, and several example applications follow in next section IV.

C. Choices for the Definition of Molecular Fragments. So far, every base has been chosen as a fragment, and the CT parameters have been calculated for sets of single bases. This is justified because the HOMO of Watson−Crick hydrogen-bonded base pairs is always localized on the purine base. As shown in Figure 3, the CT integrals do not differ significantly if whole Watson−Crick pairs GC and AT are treated as fragments, in comparison to the choice of single bases as fragments.

We systematically benchmarked various possibilities to calculate the CT integrals. (i) First of all, they can be computed for fragments consisting of single bases in the gas phase using the Hamiltonian in eq 13 to compute T_{ij}, or (ii) by choosing the same fragment in the gas phase but using the Hamiltonian in eq 14, or (iii) by computing the single base fragment MO in the presence of external charges and using the Hamiltonian in eq 14, or finally, (iv) by using a fragment consisting of the Watson−Crick dimer in the absence or presence of external charges (options iv-1 and iv-2, respectively). The most exact schemes (iv), which include most of the environmental effects already in the initial QM calculation, require the treatment of whole base pairs, leading to the computational complexity increased by a factor of 8, compared to schemes (i)−(iii), due to the doubled fragment size and the $O(N^3)$ scaling of SCC-DFTB.

The CT integrals evaluated for FOs determined by these approaches are presented in Table 3. Interestingly, the effect of hydrogen bonding is captured already by the external point charge calculation (iii), thus yielding very similar results for the couplings. On the other hand, the fragment calculations

TABLE 2: CT Integrals T_{ij} and T_{ij}' for the Intrastrand Hole Transfer in 5′-XY-3′ and 5′-YX-3′ (in the configuration with twist = 36° and rise = 3.38 Å), in Comparison with HF-KTA[65] and CAS-PT2 Values[67] (eV), and DFT values (J and J')[39]

	5′-XY-3′						5′-YX-3′					
X Y	T_{ij}	T_{ij}'	HF	CAS-PT2	J	J'	T_{ij}	T_{ij}'	HF	CAS-PT2	J	J'
A A	0.013	0.008	0.030	0.004	0.038	0.004						
C C	0.031	0.026	0.041	–	0.042	0.022						
G G	0.087	0.061	0.084	0.051	0.119	0.053						
T T	0.167	0.093	0.158	–	0.180	0.072						
A C	0.044	0.030	0.061	–	0.091	0.042	0.010	0.005	0.029	–	0.008	0.002
A G	0.059	0.037	0.049	0.044	0.013	0.010	0.080	0.052	0.089	0.036	0.186	0.077
A T	0.057	0.028	0.105	–	0.157	0.063	0.116	0.064	0.086	–	0.068	0.031
C G	0.044	0.031	0.042	–	0.026	0.009	0.091	0.057	0.110	–	0.295	0.114
C T	0.044	0.033	0.100	–	0.161	0.055	0.074	0.052	0.076	–	0.066	0.028
G T	0.100	0.049	0.137	0.081	0.334	0.141	0.123	0.070	0.085	0.061	0.044	0.018

performed for isolated bases (i) and (ii) cause sizable deviations in some cases.

However, then, once the fragments were calculated (step 1), the CT integrals were found not to be influenced by the electric field induced by the neighboring bases, as can be seen from the comparison of schemes (i) and (ii) or schemes (iv-1) and (iv-2). Therefore, the use of eqs 13 or 14 does not make a significant difference for the calculation of the couplings. (Note that this does not hold in any way for the on-site energies ϵ_i!) Therefore, single nucleobases can be chosen as fragments without loss of accuracy, as long as the fragments are polarized by the MM charges from the environment.

In summary, we find a very good agreement of IPs calculated using the ΔSCF approach and the SCC-DFTB Hamiltonian (using the standard basis) with experimental data. The calculation of the diagonal terms ϵ_i as the HOMO energy is computationally much more efficient but requires some care. The HOMO energies given by DFT-GGA exhibit a too-close energetic spacing, which may lead to orbital swapping due to geometry changes. The calculation of FOs and HOMO energies in the presence of MM point charges Q_A remedies this problem. Care should still be taken, and an analysis should be performed to check this, as the orbital swapping may not be ruled out entirely. Therefore, we propose to compute the on-site energies using the DFTB standard basis in the presence of external point charges. For the calculation of CT matrix elements, we use a slightly less confined basis set. With this basis set, the CT matrix elements match the values yielded by more accurate methods very well. A similar approach is also used to calculate the AO matrix elements of DFTB; the $H_{\mu\nu}$ values (eq 12) are calculated using the compressed, standard DFTB basis as the on-site elements ϵ_i are calculated using the free atomic wave functions.[76]

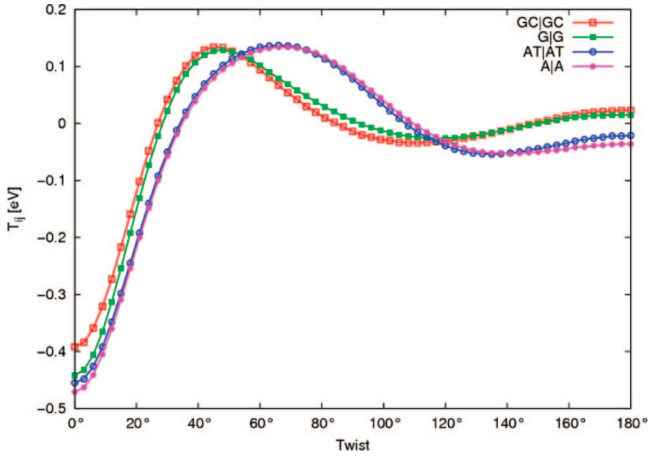

Figure 3. Comparison of CT integrals for different FO schemes; the GC/CG and AT/AT curves show the twist dependence of the T_{ij} integrals when the WC pairs GC and AT are treated as fragments, while the G/G and A/A curves were calculated as above, using the single bases A and G as fragments.

TABLE 3: CT Integrals (eV) Calculated Using Various Fragment Definitions, with and without External Charges; For the Notation, See Figure 4

	fragment definition				
hopping type	i	ii	iii	iv-1	iv-2
A|A	0.015	0.013	0.015	0.019	0.015
A/G	0.040	0.039	0.037	0.038	0.044
A|G	0.078	0.078	0.053	0.051	0.045
A/A	0.063	0.060	0.068	0.074	0.080
G\A	0.009	0.010	0.003	0.011	0.015
G\G	0.027	0.023	0.048	0.061	0.066
G|A	0.065	0.058	0.094	0.108	0.108
G/G	0.036	0.037	0.033	0.032	0.037
G|G	0.084	0.077	0.091	0.101	0.097
A\A	0.078	0.077	0.077	0.068	0.070

IV. Applications

A. CT Integrals for Relative Base Conformations: A- and B-DNA Conformation. In the course of time, the DNA bases assume different relative configurations, described, for example, by the helical parameters twist, rise, roll, slide, and so forth.[83] We have studied the dependence of CT integrals on the rise and the twist in detail. Cytosine and thymine hardly contribute to the CT process due to their large IP (see Table 1), and therefore, the coupling between adenine and/or guanine bases is likely to determine the CT rate. Figure 5 shows the CT integral for the relevant base pairs AA, GG, GA, and AG. The AA coupling assumes minimal values around the twist of 34°, a value typical for the B-DNA conformation, while the other combinations assume minima at the twist below 30°, which is close to the A-DNA conformation. In addition, these plots show that there may be non-negligible couplings even for quite large values of the rise; therefore, it is the fluctuation in twist rather than that in rise that is responsible for large variance in the CT integrals in the DNA dynamics.

To study the dependence of CT integrals on the overall DNA structure in more detail, we constructed ideal A- and B-DNA structures using the program 3DNA.[84] In accordance with the

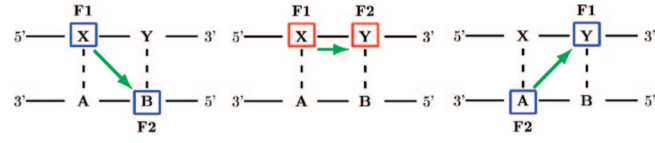

Figure 4. X/B ≡ B/X denotes the interstrand 5′−5′ hopping (left), X|Y the intrastrand hopping (center) (caution: X|Y and Y|X differ unless X = Y), and Y\A denotes the interstrand 3′−3′ hopping (right).

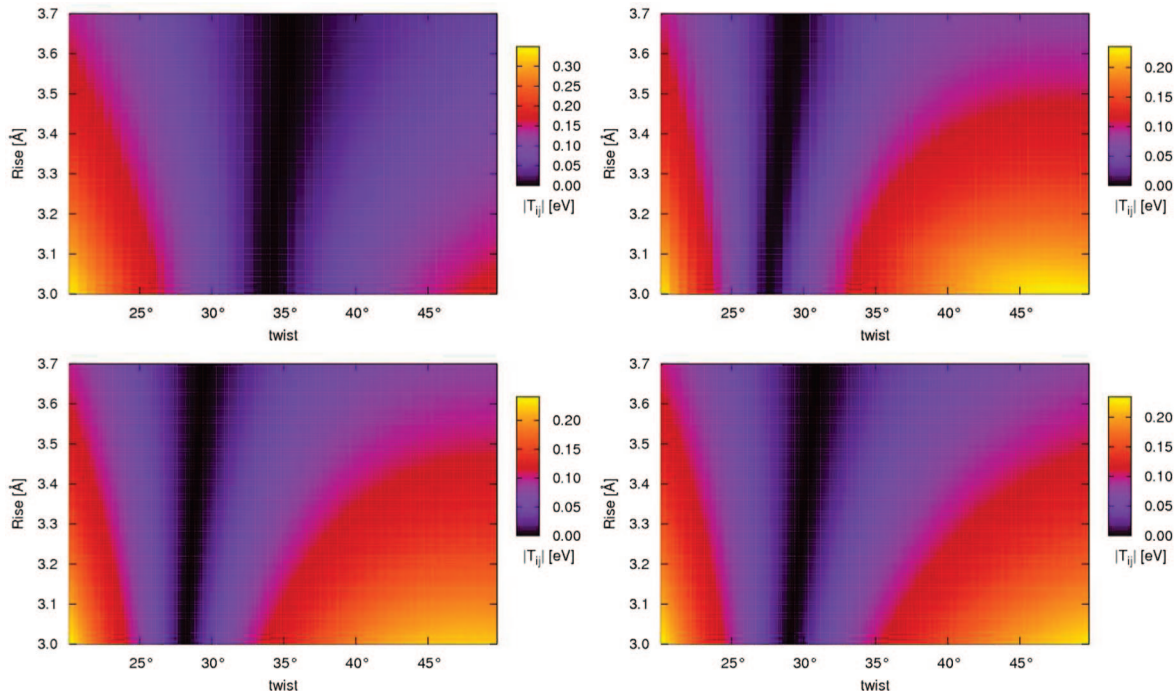

Figure 5. CT integral ($|T_{ij}|$) for intrastrand hole transfer in the base pair steps AA (top left), GG (top right), GA (bottom left), and AG (bottom right); twist = 20–50°, rise = 3.0–3.7 Å.

TABLE 4: T_{ij} and T_{ij}' (eV) in DNA Base Pair Steps Calculated with DFTB for B-DNA (twist = 36° and rise = 3.38 Å) as well as for A-DNA (twist = 32°, rise = 3.20 Å, roll = 12° and slide = −1.5 Å; parameters taken from refs 94 and 95) with Intrastrand Coupling if Both Purine Bases Are Located in One Strand and InterStrand Coupling Otherwise

		5′-XY-3′		5′-YX-3′				5′-XY-3′		5′-YX-3′	
B-DNA	X Y	T_{ij}	T_{ij}'	T_{ij}	T_{ij}'	A-DNA	X Y	T_{ij}	T_{ij}'	T_{ij}	T_{ij}'
		intrastrand						intrastrand			
	A A	0.019	0.019				A A	0.118	0.078		
	G G	0.101	0.072				G G	0.002	0.006		
	A G	0.051	0.035	0.108	0.071		A G	0.069	0.046	0.021	0.021
		interstrand						interstrand			
	G C	0.032	0.020	0.084	0.051		G C	0.005	0.001	0.095	0.057
	A T	0.074	0.047	0.068	0.032		A T	0.032	0.018	0.211	0.118
	A C	0.038	0.025	0.011	0.011		A C	0.015	0.006	0.133	0.080

data presented above, the poly(AA)−intrastrand couplings in Table 4 are quite small compared to the poly(GG), poly(AG), and poly(GA) (5′-YX-3′). Interestingly, the interstrand values are still quite large for both the A- and B-form as shown in Table 4. On the other hand, the GG coupling vanishes in the A-form, while the AA couplings take quite large values, as can also be inferred from Figure 5.

B. xDNA and G4 Structures. Because of a growing consensus that double-stranded DNA may not be the optimal candidate for molecular electronics applications (REF), there is research going on to apply various DNA derivatives in nanoelectronic applications. For instance, the G4-DNA wires are formed by stacked guanine quartets (see Figure 6). These DNA species may be structurally stiffer and more resistant to surface forces than the double helix, while keeping the self-assembling properties of the latter.[85] Evidence of polarizability of long G4-DNA molecules, as measured by electrostatic force microscopy, has been recently demonstrated by Porath and co-workers.[85] In contrast, double-stranded DNA molecules coadsorbed on mica were electrically silent. This firmly suggests that G4-DNA may be a better conductor than double-stranded DNA.

We calculated the CT integrals for such a structure dependent on the torsional angle ("twist") between two quartets; see Figure 7. Although the observed T_{ij} is not distinctly larger than in the case of normal DNA (no matter if A- or B-like), the larger stability of G4-DNA may lead to a different dynamical behavior, thus making the CT integrals maintain larger values.

Another interesting alternative to natural DNA is the so-called xDNA, where an extra aromatic ring is inserted into every base molecule; see Figure 6. The spatial extension of the bases increases stacking interactions, which in turn leads to higher

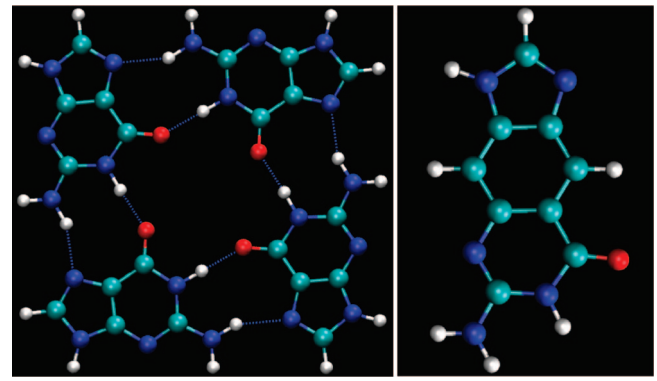

Figure 6. The structure of the guanine quartet (G4, left) and extended guanine (xG, right).

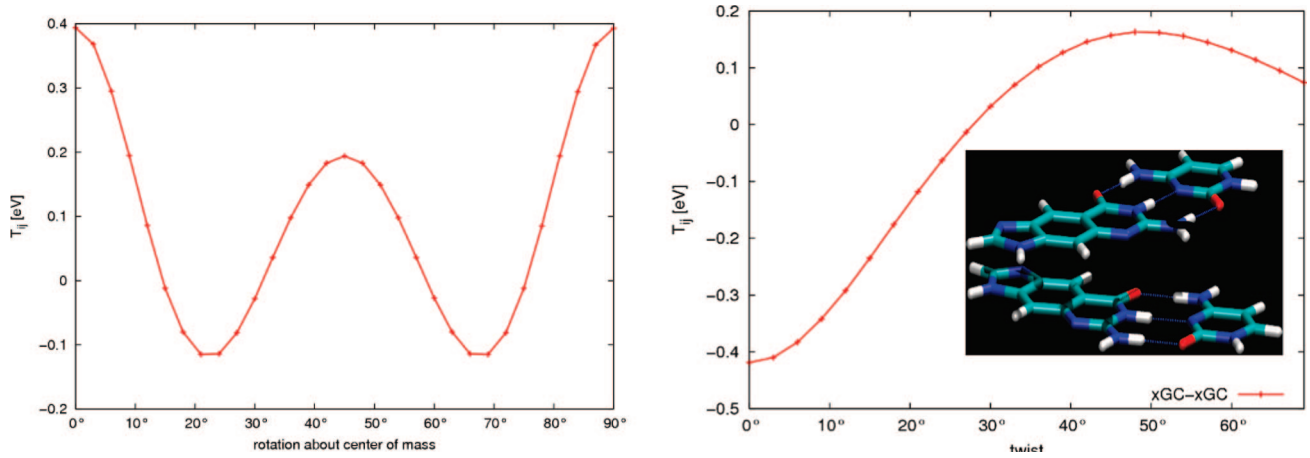

Figure 7. CT integral in a pair of guanine quartets (left) and in stacked xDNA base pairs (right); dependence on the torsional angle.

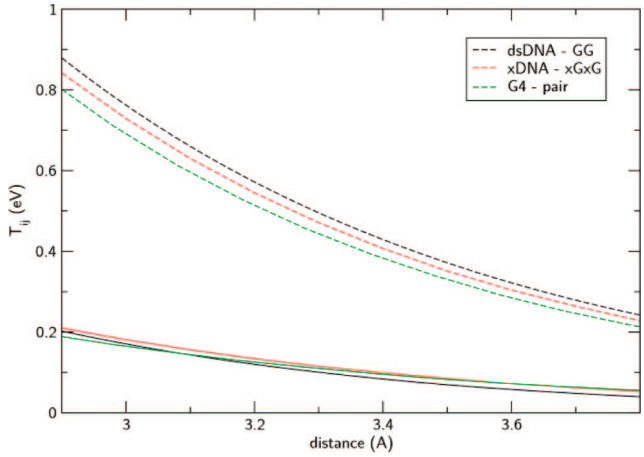

Figure 8. CT integral dependence on the distance of nucleobases in DNA and xDNA and of guanine quartets. Shown are data for the twist/torsional angles of 0° (broken lines) and 36° (solid lines).

thermodynamic stability.[86,87] Here, we studied the dependence of T_{ij} on the torsion angle as well; see Figure 7. Again, the CT integrals do not exceed those for natural A-/B-DNA markedly (compare with Figure 2).

Also, we quantified the dependence of the CT integral on the vertical distance between base pairs in natural dsDNA and xDNA and on that between two G4 units; see Figure 8. All curves follow a similar trend, falling off with the increasing distance.

At the first sight, it is surprising that the electronic π systems in these extended structures do not exhibit a markedly increased overlap, which would result in larger CT couplings. The observed higher polarizability of G4[85] may then only be related to a higher structural stability, as reported for xDNA.[87] However, these structures may additionally assume different average structures, for example, if sampled in a MD simulation. This would change the average CT couplings significantly. Indeed, first MD simulations indicate a slight difference between xDNA and natural B-DNA; the xDNA has slightly smaller values of rise and twist.[88] Whether this leads to a different dynamical behavior and larger average values of CT couplings compared to those of natural DNA is the subject of ongoing investigation in our laboratory.

C. Calculation of CT Characteristics along MD Trajectories. The examples described so far indicate that the CT parameters depend sensitively on the structure (see, e.g., also ref 53). Therefore, the use of static structures may provide only a limited insight into the charge-transfer process in DNA and its derivatives. The evaluation of CT parameters along molecular dynamics trajectories has shown this in detail.[54,58] DNA species of different sequence assume different conformations in solution, and the structural fluctuations may lead to a completely different picture when the dynamics of DNA is considered. Also, neglecting the effect of solvent structural fluctuations renders an incomplete description of the problem.

As shown above, both IPs and CT integrals calculated with SCC-DFTB agree nicely with those stemming from higher-level methods, and therefore, we are going on with using this method in a multiscale scheme together with MD simulations. We performed classical MD simulations of a solvated poly(GA) undecamer using the AMBER-parm99 force field with the parmBSC0 correction,[89,90] by means of the GROMACS software package.[91]

Initially, we set the time step to 0.1 fs and evaluated on-site energies and CT integrals for snapshots recorded in every MD step. Figure 9 (left) shows the IP of two purine bases calculated along a 100 fs interval of this MD simulation. The IPs are calculated by means of the ΔSCF procedure with both DFT (PBE functional using the TurboMole package)[92] and SCC-DFTB using the standard basis set.[96]

The SCC-DFTB values agree nicely with the DFT ones, showing identical time dependence and also the same magnitude of fluctuations. The same is true about the Kohn−Sham eigenvalue of HOMO; see Figure 9 (right). The difference of DFTB and PBE values takes a constant small value of 0.15 eV for guanine and 0.06 eV for adenine. As noted above, the Kohn−Sham energies represent a poor approximation of the absolute IP values; however, as shown in Figure 9, they follow the fluctuations of real IPs quite accurately. Since it is only such relative energetics of a hole on the nucleobases that is of importance, even this simplified approach can be used in the applications.

The time course of T_{ij} in the poly(GA) undecamer, calculated with the 8−7 DFTB basis set, is presented in Figure 10. All T_{ij}'s exhibit large fluctuations and deviate substantially from the values for poly(GA) in the ideal B-DNA conformation (0.051 eV for the AG and 0.108 eV for the GA base pair step; cf. Table 4). On the short time scale presented in Figure 10, the individual base pair steps assume quite different values of T_{ij}, as reported before.[54] This is due to the conformation not exactly corresponding to the ideal B-DNA structure (rms deviation around 2 Å) and, more importantly, the large structural changes in general.

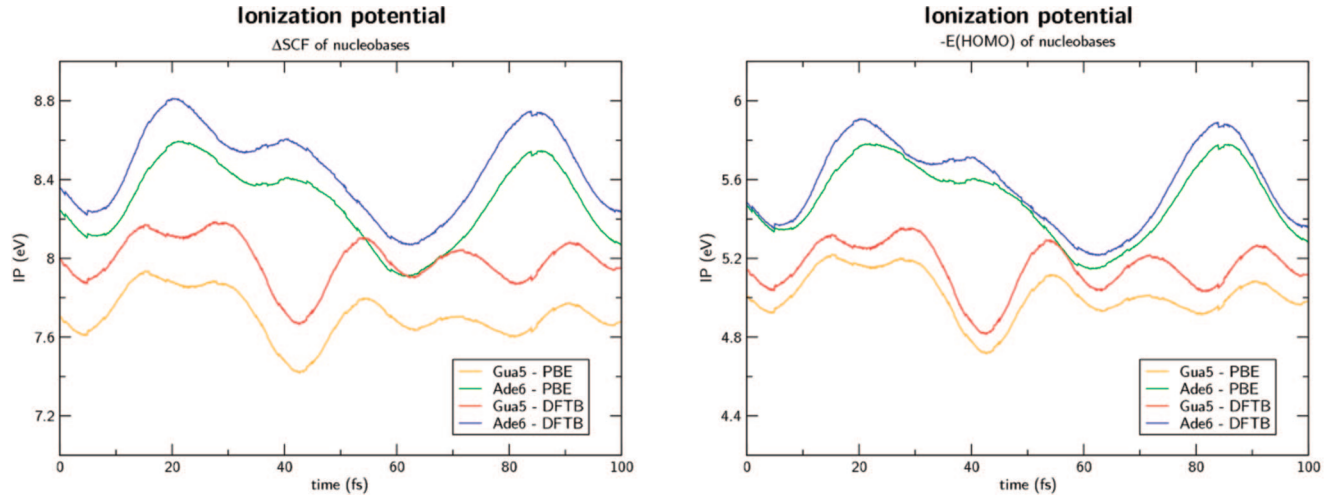

Figure 9. The IP of a guanine and an adenine in a poly(GA) undecamer calculated for a 100 fs MD trajectory as the ΔSCF (left) and Kohn−Sham energy (ϵ_{HOMO}, right).

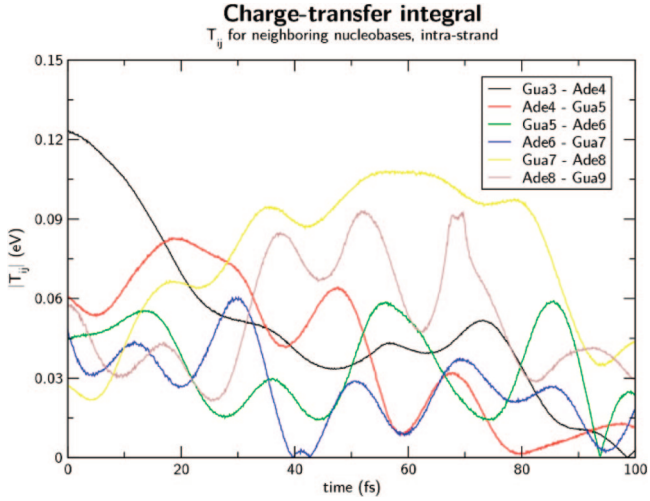

Figure 10. The CT integral in a poly(GA) undecamer calculated for a 100 fs MD trajectory.

The examples presented above illustrate the typical behavior of CT characteristics, which are to be observed in MD simulations of DNA; the fastest oscillations occur on the multifemtosecond scale. It seems obvious that, rather than 0.1 fs, the choice of 1 fs for the time step makes sure both sufficient sampling (if required) and acceptable efficiency.

To gain a more profound insight, we calculated the mean values of CT integrals in the course of a multinanosecond MD simulation. In such case, we simulated the DNA with the usual time step of 2 fs and performed the calculation of fragments and the complex, for example, every 1 ps to obtain a set of data that is both sufficiently large and statistically independent. In the following example, we analyze a 10 ns unrestrained simulation of the poly(GA) undecamer in that way. For the calculated on-site energies and CT integrals, see Table 5. We see that the HOMO level of adenines lies roughly 0.4 eV above that of guanines; also, HOMOs at the nucleobases in the middle of the strand lie higher than those at the ends. The amplitude of their fluctuation is on the order of 0.4 eV, in accordance with the previous report of Voityuk et al.[58] The main feature of computed CT integrals worth mentioning is their heavy fluctuation, expressed by the standard deviation reaching the magnitude of the mean value. Most interestingly, the difference between the GA and AG steps found for the "ideal" B-DNA structure is completely washed out. Both base pair steps fluctuate around a mean value of 0.05−0.06 eV.

TABLE 5: On-Site Energies and CT Integrals in the Poly(GA) Undecamer and Average Values and Standard Deviations from a 100 ps MD simulation[a]

base	ϵ_{HOMO} (eV)	base pair step	T_{ij} (eV)
Gua3	5.89 ± 0.44	G3|A4	0.055 ± 0.049
Ade4	6.44 ± 0.37	A4|G5	0.051 ± 0.045
Gua5	6.13 ± 0.36	G5|A6	0.053 ± 0.046
Ade6	6.53 ± 0.35	A6|G7	0.053 ± 0.044
Gua7	6.14 ± 0.38	G7|A8	0.064 ± 0.052
Ade8	6.44 ± 0.38	A8|G9	0.069 ± 0.054
Gua9	5.88 ± 0.43		

[a] The standard DFTB basis set was used to obtain on-site energies, while the calculation of T_{ij} was performed with the 8−7 basis set.

The efficiency of the DFTB-based FO scheme allows computation of CT parameters for long MD trajectories. The analysis of one MD frame, where the FO calculations are performed, took three seconds on a mainstream desktop PC, that is, it is possible to analyze multinanosecond MD for the purpose of statistical processing or to calculate the CT-related quantities with dense sampling along MD trajectories reaching a nanosecond.

V. Conclusions

In summary, we have presented a multiscale model to study the hole transfer in DNA. The model is based on the SCC-DFTB matrix elements and a fragment-orbital (FO) approach. This FO approach requires the quantum mechanical problem to be solved for the individual nucleobases only. Therefore, the method exhibits an effective linear scaling with the increasing system size. As has been shown, the on-site energies ϵ_i and off-diagonal CT integrals T_{ij} compare very well with higher-level approaches (DFT, CAS-PT2) but in a calculation orders of magnitude faster than with HF or DFT methods. The QM/MM framework incorporates environmental effects in a realistic way, and the coupling to classical MD simulation allows for the inclusion of dynamical effects. These may be the statistical averaging of structures or the calculation of time-dependent events, for example, the solution of the time-dependent Schrödinger equation using the hole Hamiltonian T_{ij} to simulate the hole migration. Such methodology should enable one to unravel

the mechanisms of charge transfer in DNA or related materials in molecular detail.

The SCC-DFTB FO model is a quite general scheme which should be applicable to electron-transfer (ET) reactions in proteins and other materials like, for example, organic crystals. Definitely, this requires careful and system-specific testing. Since environmental effects and structural fluctuations can be expected to be of similar importance for ET reactions in other materials, it seems inevitable to use a method based on a combination of classical MD simulations and electronic structure calculations in a multiscale approach, which can take these effects into account properly.

Acknowledgment. This work was supported by Deutsche Forschungsgemeinschaft (Project DFG-EL 206/5-1).

Supporting Information Available: The energy and symmetry character of the three highest occupied MOs in DNA bases calculated with DFTB as well as HF and various DFT functionals for various nucleobase geometries. This material is available free of charge via the Internet at http://pubs.acs.org.

References and Notes

(1) Schuster, G. B., Ed. *Long-Range Charge Transfer in DNA I-II: Topics in Current Chemistry*; Springer: Heidelberg, 2004.
(2) Boon, E. M.; Livingston, A. L.; Chmiel, N. H.; David, S. S.; Barton, J. K. *Proc. Natl. Acad. Sci. U.S.A.* **2003**, *100*, 12543.
(3) Holman, M. R.; Ito, T.; Rokita, S. E. *J. Am. Chem. Soc.* **2007**, *129*, 6.
(4) Endres, R. G.; Cox, D. L.; Singh, R. R. P. *Rev. Mod. Phys.* **2004**, *76*, 195.
(5) Porath, D.; Lapidot, N.; Gomez-Herrero, J. In *Introducing Molecular Electronics*, Lecture Notes in Physics 680; Cuniberti, G., Fagas, G., Richter, K., Eds.; Springer: Berlin, Germany, 2005; p 411.
(6) Porath, D.; Cuniberti, G.; Di Felice, R. *Top. Curr. Chem.* **2004**, *237*, 183.
(7) Eley, D. D.; Spivey, D. I. *Trans. Faraday Soc.* **1962**, *58*, 411.
(8) de Pablo, P. J.; Moreno-Herrero, F.; Colchero, J.; Herrero, J. G.; Herrero, P.; Baro, A. M.; Ordejon, P.; Soler, J. M.; Artacho, E. *Phys. Rev. Lett.* **2000**, *85*, 4992.
(9) Lewis, J.; Cheatham, T.; Starikov, E. B.; Wang, H.; Sankey, O. F. *J. Phys. Chem. B* **2003**, *107*, 2581.
(10) Giese, B.; Amaudrut, J.; Köhler, A.-K.; Spormann, M.; Wessely, S. *Nature* **2002**, *412*, 318.
(11) Giese, B. *Top. Curr. Chem.* **2004**, *236*, 27.
(12) Priyadarshy, S.; Risser, S. M.; Beratan, D. N. *J. Phys. Chem.* **1996**, *100*, 17678.
(13) Jortner, J.; Bixon, M.; Langenbacher, T.; Michel-Beyerle, M. E. *Proc. Natl. Acad. Sci. U.S.A* **1998**, *95*, 12759.
(14) Priyadarshy, S.; Beratan, D. N.; Risser, S. M. *Int. J. Quantum Chem.* **1996**, *60*, 1789.
(15) Tong, G. S. M.; Kurnikov, I. V.; Beratan, D. N. *J. Phys. Chem. B* **2002**, *106*, 2381.
(16) Lewis, F. D.; Liu, J.; Weigel, W.; Rettig, W.; Kurnikov, I. V.; Beratan, D. N. *Proc. Natl. Acad. Sci. U.S.A.* **2002**, *99*, 12536.
(17) Olofsson, J.; Larsson, S. *J. Phys. Chem. B* **2001**, *105*, 10398.
(18) Hall, D. B.; Holmlin, E.; Barton, J. K. *Nature* **1996**, *382*, 731.
(19) Hall, D. B.; Barton, J. K. *J. Am. Chem. Soc.* **1997**, *119*, 5045.
(20) Gasper, S. M.; Schuster, G. B. *J. Am. Chem. Soc.* **1997**, *119*, 12762.
(21) Giese, B.; Wessely, S.; Spormann, M.; Lindemann, U.; Meggers, E.; Michel-Beyerle, M. E. *Angew. Chem., Int. Ed.* **1999**, *38*, 996.
(22) Meggers, E.; Michel-Beyerle, M. E.; Giese, B. *J. Am. Chem. Soc.* **1998**, *120*, 12950.
(23) Ly, D.; Kan, Y.; Armitage, B.; Schuster, G. B. *J. Am. Chem. Soc.* **1996**, *118*, 8747.
(24) Grozema, F. C.; Berlin, Y. A.; Siebbeles, L. D. A. *J. Am. Chem. Soc.* **2000**, *122*, 10903.
(25) Bixon, M.; Jortner, J. *J. Phys. Chem. B* **2000**, *104*, 3906.
(26) Bixon, M.; Jortner, J. *J. Am. Chem. Soc.* **2001**, *123*, 12556.
(27) Berlin, Y. A.; Burin, A. L.; Ratner, M. A. *J. Am. Chem. Soc.* **2001**, *123*, 260.
(28) Berlin, Y. A.; Burin, A. L.; Ratner, M. A. *Chem. Phys.* **2002**, *275*, 61.
(29) Bixon, M.; Jortner, J. *Chem. Phys.* **2002**, *281*, 393.
(30) Bixon, M.; Jortner, J. *Chem. Phys.* **2006**, *326*, 252.
(31) Lewis, F. D.; Zhu, H.; Daublain, P.; Fiebig, T.; Raytchev, M.; Wang, Q.; Shafirovich, V. *J. Am. Chem. Soc.* **2006**, *128*, 791.
(32) Lewis, F. D.; Zhu, H.; Daublain, P.; Cohen, B.; Wasielewski, M. R. *Angew. Chem., Int. Ed.* **2006**, *45*, 7982.
(33) Lewis, F. D.; Daublain, P.; Cohen, B.; Vura-Weis, J.; Shafirovich, V.; Wasielewski, M. R. *J. Am. Chem. Soc.* **2007**, *129*, 15130.
(34) Hush, N. S.; Cheung, A. S. *Chem. Phys. Lett.* **1975**, *34*, 11.
(35) Orlov, V. M.; Smirnov, A. N.; Varshavsky, Y. M. *Tetrahedron Lett.* **1976**, *17*, 4377.
(36) Steenken, S.; Jovanovic, S. V. *J. Am. Chem. Soc.* **1997**, *119*, 617.
(37) Newton, M. D. *Chem. Rev.* **1991**, *91*, 767.
(38) Grozema, F. C.; Siebbeles, L. D. A.; Berlin, Y. A.; Ratner, M. A. *ChemPhysChem* **2002**, *3*, 536.
(39) Senthilkumar, K.; Grozema, F. C.; Guerra, C. F.; Bickelhaupt, F. M.; Lewis, F. D.; Berlin, Y. A.; Ratner, M. A.; Siebbeles, L. *J. Am. Chem. Soc.* **2007**, *127*, 14894.
(40) Conwell, E. *Top. Curr. Chem.* **2004**, *237*, 73.
(41) Conwell, E.; Park, J.; Choi, H. *J. Phys. Chem. B* **2005**, *109*, 9760.
(42) Cramer, T.; Krapf, S.; Koslowski, T. *J. Phys. Chem. B* **2004**, *108*, 11812.
(43) Cuniberti, G.; Macia, E.; Rodriguez, A.; Roemer, R. A. In *Charge Migration in DNA: Perspectives from Physics, Chemistry and Biology*; Chakraborty, T., Ed.; Springer: Berlin, Germany, 2007; p 1.
(44) Gutierrez, R.; Cuniberti, G. In *NanoBioTechnology: BioInspired Device and Materials of the Future*; Shoseyov, O., Levy, I., Eds.; Humana Press: Clifton, NJ, 2007; p 107.
(45) Cramer, T.; Steinbrecher, T.; Labahn, A.; Koslowski, T. *Phys. Chem. Chem. Phys.* **2004**, *7*, 4039.
(46) Medvedev, E. S.; Stuchebrukhov, A. A. *J. Chem. Phys.* **1997**, *107*, 3821.
(47) Skourtis, S. S.; Archontis, G.; Xie, Q. *J. Chem. Phys.* **2001**, *115*, 9444.
(48) Troisi, A.; Nitzan, A.; Ratner, M. A. *J. Chem. Phys.* **2003**, *119*, 5782.
(49) Troisi, A.; Ratner, M. A.; Zimmt, M. B. *J. Am. Chem. Soc.* **2004**, *126*, 2215.
(50) Skourtis, S. S.; Balabin, I. A.; Kawatsu, T.; Beratan, D. N. *Proc. Natl. Acad. Sci. U.S.A.* **2005**, *102*, 3552.
(51) Nishioka, H.; Kimura, A.; Yamato, T.; Kawatsu, T.; Kakitani, T. *J. Phys. Chem. B* **2005**, *109*, 15621.
(52) Prytkova, T. R.; Kurnikov, I. V.; Beratan, D. N. *Science* **2007**, *315*, 622.
(53) Voityuk, A.; Siriwong, K.; Roesch, N. *Phys. Chem. Chem. Phys.* **2001**, *3*, 5421.
(54) Troisi, A.; Orlandi, G. *J. Phys. Chem. A* **2002**, *106*, 2093.
(55) Voityuk, A. *Chem. Phys. Lett.* **2006**, *439*, 162.
(56) Volobuyev, M.; Saint-Martin, H.; Adamowicz, L. *J. Phys. Chem. B* **2007**, *111*, 11083.
(57) Yamada, H.; Starikow, E. B.; Henning, D. *Eur. Phys. J. B* **2007**, *59*, 185.
(58) Voityuk, A.; Siriwong, K.; Roesch, N. *Angew. Chem., Int. Ed.* **2004**, *43*, 624.
(59) O'Neill, M. A.; Barton, J. K. *Top. Curr. Chem.* **2004**, *236*, 67.
(60) Schuster, G. B.; Landmann, U. *Top. Curr. Chem.* **2004**, *236*, 139.
(61) O'Neill, M. A.; Barton, J. K. *J. Am. Chem. Soc.* **2004**, *126*, 11471.
(62) Barnett, R. N.; Cleveland, C. L.; Joy, A.; Landman, U.; Schuster, G. B. *Science* **2001**, *294*, 567.
(63) Mantz, Y. A.; Gervasio, F. L.; Laino, T.; Parrinello, M. *Phys. Rev. Lett.* **2007**, *99*, 058104.
(64) Roesch, N.; Voityuk, A. *Top. Curr. Chem.* **2004**, *237*, 37.
(65) Voityuk, A. A.; Roesch, N.; Bixon, M.; Jortner, J. *J. Phys. Chem. B* **2000**, *104*, 9740.
(66) Voityuk, A. A.; Jortner, J.; Bixon, M.; Roesch, N. *J. Chem. Phys.* **2001**, *114*, 5614.
(67) Blancafort, L.; Voityuk, A. *J. Phys. Chem. A* **2006**, *110*, 6426.
(68) Troisi, A.; Orlandi, G. *Chem. Phys. Lett.* **2001**, *344*, 509.
(69) Rak, J.; Makowska, J.; Voityuk, A. *Chem. Phys.* **2006**, *325*, 567.
(70) Maragakis, P.; Barnett, R. L.; Kaxiras, E.; Elstner, M.; Frauenheim, T. *Phys. Rev. B* **2002**, *66*, 2411041.
(71) Barnett, R. L.; Maragakis, P.; Turner, A.; Fyta, M.; Kaxiras, E. *J. Mater. Sci.* **2007**, *42*, 8894.
(72) Mehrez, H.; Anantram, M. P. *Phys. Rev. B* **2005**, *71*, 115405.
(73) Senn, H. M.; Thiel, W. *Curr. Opin. Chem. Biol.* **2007**, *11*, 182.
(74) Elstner, M.; Porezag, D.; Jungnickel, G.; Elsner, J.; Haugk, M.; Frauenheim, T.; Suhai, S.; Seifert, G. *Phys. Rev. B* **1998**, *58*, 7260.
(75) Loewdin, P. O. *J. Chem. Phys.* **1950**, *18*, 365.
(76) Porezag, D.; Frauenheim, T.; Köhler, T.; Seifert, G.; Kaschner, R. *Phys. Rev. B* **1995**, *51*, 12947.
(77) Elstner, M. *Theor. Chem. Acc.* **2006**, *116*, 316.
(78) Seifert, G. *J. Phys. Chem. A* **2007**, *111*, 5609.
(79) Elstner, M. *J. Phys. Chem. A* **2007**, *111*, 5614.
(80) Cui, Q.; Elstner, M.; Kaxiras, E.; Frauenheim, T.; Karplus, M. *J. Phys. Chem. B* **2001**, *105*, 569.

(81) Frisch, M. J. Trucks, G. W.; Schlegel, H. B.; Scuseria, G. E.; Robb, M. A.; Cheeseman, J. R.; Montgomery, J. A.; Jr. Vreven, T.; Kudin, K. N.; Burant, J. C.; Millam, J. M.; Iyengar, S. S.; Tomasi, J.; Barone, V.; Mennucci, B.; Cossi, M.; Scalmani, G.; Rega, N.; Petersson, G. A.; Nakatsuji, H.; Hada, M.; Ehara, M.; Toyota, K.; Fukuda, R.; Hasegawa, J.; Ishida, M.; Nakajima, T.; Honda, Y.; Kitao, O.; Nakai, H.; Klene, M.; Li, X.; Knox, J. E.; Hratchian, H. P.; Cross, J. B.; Bakken, V.; Adamo, C.; Jaramillo, J.; Gomperts, R.; Stratmann, R. E.; Yazyev, O.; Austin, A. J.; Cammi, R.; Pomelli, C.; Ochterski, J. W.; Ayala, P. Y.; Morokuma, K.; Voth, G. A.; Salvador, P.; Dannenberg, J. J.; Zakrzewski, V. G.; Dapprich, S.; Daniels, A. D.; Strain, M. C.; Farkas, O.; Malick, D. K.; Rabuck, A. D.; Raghavachari, K.; Foresman, J. B.; Ortiz, J. V.; Cui, Q.; Baboul, A. G.; Clifford, S.; Cioslowski, J.; Stefanov, B. B.; Liu, G.; Liashenko, A.; Piskorz, P.; Komaromi, I.; Martin, R. L.; Fox, D. J.; Keith, T.; Al-Laham, M. A.; Peng, C. Y.; Nanayakkara, A.; Challacombe, M.; Gill, P. M. W.; Johnson, B.; Chen, W.; Wong, M. W.; Gonzalez, C.; Pople, J. A. *Gaussian 03*, revision C.02; Gaussian, Inc.: Wallingford, CT, 2004.

(82) York, D. M.; Lee, T.-S.; Yang, W. *Phys. Rev. Lett.* **1998**, *80*, 5011.

(83) Olson, W. K.; Bansal, M.; Burley, S. K.; Dickerson, R. E.; Gerstein, M.; Harvey, S. C.; Heinemann, U.; Lu, X-J.; Neidle, S.; Shakked, Z.; Sklenar, H.; Suzuki, M.; Tung, C-S.; Westhof, E.; Wolberger, C.; Berman, H. M. *J. Mol. Biol.* **2001**, *313*, 229.

(84) Lu, X.-J.; Olson, W. K. *Nucleic Acids Res.* **2003**, *31*, 5108.

(85) Cohen, H.; Sapir, T.; Borovok, N.; Molotsky, T.; Di Felice, R.; Kotlyar, A.; Porath, D. *Nano Lett.* **2007**, *7*, 981.

(86) Liu, H.; Gao, J.; Maynard, L.; Saito, Y. D.; Kool, E. T. *J. Am. Chem. Soc.* **2004**, *126*, 1102.

(87) Liu, H.; Gao, J.; Maynard, L.; Saito, Y. D.; Kool, E. T. *J. Am. Chem. Soc.* **2004**, *126*, 6900.

(88) Fuentes-Cabrera, M.; Zhao, X.; Kent, P.; Sumpter, B. G. *J. Phys. Chem. B* **2007**, *111*, 9057.

(89) Wang, J.; Cieplak, P.; Kollman, P. A. *J. Comput. Chem.* **2000**, *21*, 1049.

(90) Pérez, A.; Marchán, I.; Svozil, D.; Šponer, J.; Cheatham, T. E., III; Laughton, C. A.; Orozco, M. *Biophys. J.* **2007**, *92*, 3817.

(91) van der Spoel, D.; Lindahl, E.; Hess, B.; Groenhof, G.; Mark, A. E.; Berendsen, H. J. C. *J. Comput. Chem.* **2005**, *26*, 1701.

(92) Ahlrichs, R.; Bär, M.; Häser, M.; Horn, H.; Kölmel, C. *Chem. Phys. Lett.* **1989**, *162*, 165.

(93) Voityuk, A. A.; Jortner, J.; Bixon, M.; Roesch, N. *Chem. Phys. Lett.* **2000**, *324*, 430.

(94) Lu, X.-J.; El Hassan, M. A.; Hunter, C. A. *J. Mol. Biol.* **1997**, *273*, 681.

(95) Calladine, C. R.; Drew, H. R. *Understanding DNA; The Molecule & How it Works*; Academic Press: London, 1992.

(96) Although the nearly uncompressed basis functions (with the 8−7 basis set) lead to very good values of the off-diagonal T_{ij}, the diagonal ϵ_i are changed quite significantly, leading to larger deviations from the PBE single-particle values.

JP801486D